Applied Clay Science 258 (2024) 107478

Contents lists available at ScienceDirect

Applied Clay Science

journal homepage: www.elsevier.com/locate/clay

Research Paper

Illitization of montmorillonite in ammonium solutions under hydrothermal conditions

María Bentabol [a], Daniel Lamarca-Irisarri [b], Alexander E.S. Van Driessche [b], Peter C. Ryan [c], F. Javier Huertas [b,*]

[a] Departamento de Química Inorgánica, Cristalografía y Mineralogía, Facultad de Ciencias, Universidad de Málaga, Campus de Teatinos, 29071 Málaga, Spain
[b] Instituto Andaluz de Ciencias de la Tierra (IACT, CSIC), Avda. de las Palmeras 4, 18100 Armilla (Granada), Spain
[c] Earth and Climate Sciences, Middlebury College, Middlebury, VT 05753, USA

ARTICLE INFO

Keywords:
Illitization
NH_4-micas
Hydrothermal synthesis
Smectite
Ammonium

ABSTRACT

In diagenetic solutions, ammonium may be incorporated into smectites as an exchangeable cation and become fixed within the interlayer space of illites and other white micas. To study the potential impact of NH_4^+ on the smectite-to-illite transformation reaction, a series of hydrothermal experiments were carried out at 100, 150 and 200 °C, spanning reaction duration from 15 to 90 days, and two NH_4^+ concentrations (0.1 and 0.2 M). The solids resulting from these alteration experiments were characterized using X-ray diffraction (XRD), Fourier-transform infrared spectroscopy (FT-IR), and transmission and analytical electron microscopy (TEM and AEM). The XRD analysis revealed that, under the specified experimental conditions, smectite incorporates NH_4^+ in the structure, leading to the formation of non-swelling layers, resulting in partial transformation to illite layers and producing packets of disordered illite/smectite (I/S). In addition, a minor XRD peak at ~10 Å suggests the formation of discrete illite crystals. The FTIR spectra demonstrated the uptake of NH_4^+, with deformation bands observed at 1400 and 1430 cm^{-1}, corresponding to exchangeable NH_4^+ in smectite and fixed NH_4^+ in high-charge layers, respectively. TEM analysis revealed that smectite particles exhibited wavy stacks comprising a few layers with abundant defects and lateral discontinuities. The interlayer spacing in these particles ranged from 12 to 15 Å and became thinner and more plate-like with increasing temperature and time. Moreover, they contained inclusions of 10–10.3 Å layers, either as discrete layers or in packets of several layers, indicating the formation of disordered mixed-layer illite-smectite. Lateral transitions from 12 to 15 Å to 10 Å layers were frequently observed and interpreted as reaction fronts due to local rearrangement. At 150 and 200 °C, isolated packets of 10 Å layers were identified as discrete illite crystals that precipitated directly from solution. Analysis of the chemical composition of individual particles revealed an increase in octahedral charge (Mg^{VI} for Al^{VI} substitution) in smectite particles, followed by increase in tetrahedral charge in I/S particles. Interlayer NH_4^+ played a stabilizing role in the high-charge layers and favored the smectite-to-illite conversion process.

1. Introduction

The interaction between mineral and solutions includes processes such as adsorption, dissolution and precipitation. These processes play a critical role in regulating the exchange of elements between rocks, sediments, and the fluids found within the Earth's crust, hydrosphere, and biosphere. These reactions can govern the biogeochemical cycles of elements, including mineral formation and alteration, retention of pollutants, release of nutrients, interactions with living organisms, and more. During diagenesis, several reactions induce changes in both phyllosilicates and organic matter, which, in basins associated with hydrocarbon production, lead to ammonium fixation in illite and micas (Williams and Ferrell, 1991; Środoń, 2010) and dissolution induced by organic acids (Surdam et al., 1989; Barman et al., 1992; Drever and Stillings, 1997; Lawrence et al., 2014).

Clay minerals accumulate in sedimentary basins, and changes in environmental conditions during burial, such as increasing temperature and pressure, porosity reduction, and the incorporation of new chemical

* Corresponding author.
E-mail addresses: bentabol@uma.es (M. Bentabol), dlamarca82@gmail.es (D. Lamarca-Irisarri), alexander.vd@csic.es (A.E.S. Van Driessche), pryan@middlebury.edu (P.C. Ryan), javier.huertas@csic.es (F.J. Huertas).

https://doi.org/10.1016/j.clay.2024.107478
Received 22 January 2024; Received in revised form 24 June 2024; Accepted 26 June 2024
Available online 2 July 2024

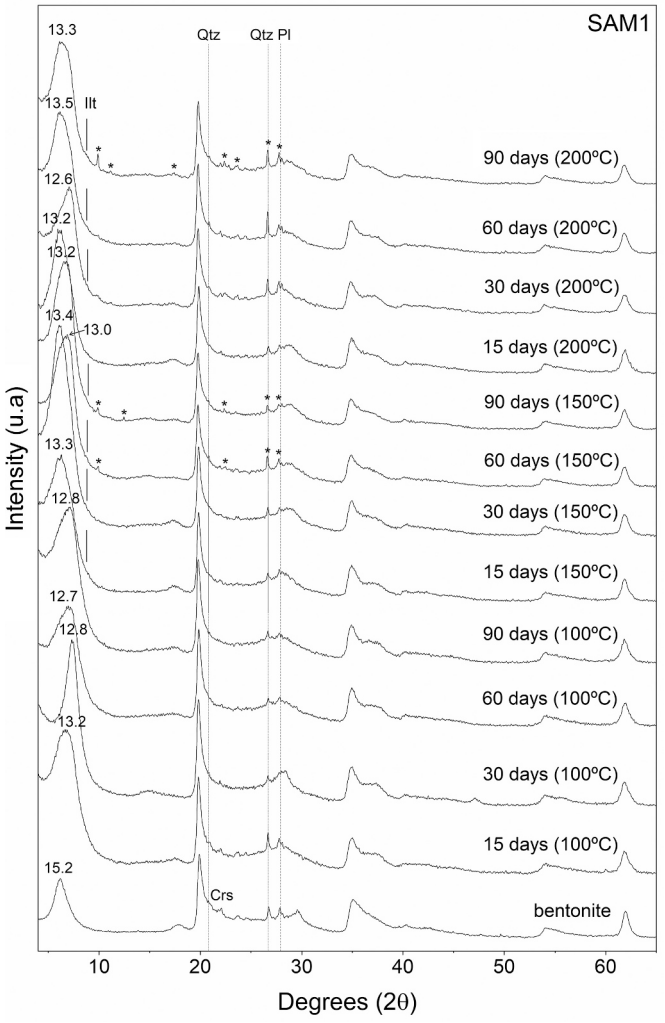

Fig. 1. XRD patterns obtained from randomly oriented mounts of starting material and solid products of reactions SAM (0.1 M) at 100, 150 and 200 °C and 15, 30, 60 and 90 days of reaction. Star: clinoptilolite, Crs: cristobalite, Ilt: illite, Qtz: quartz.

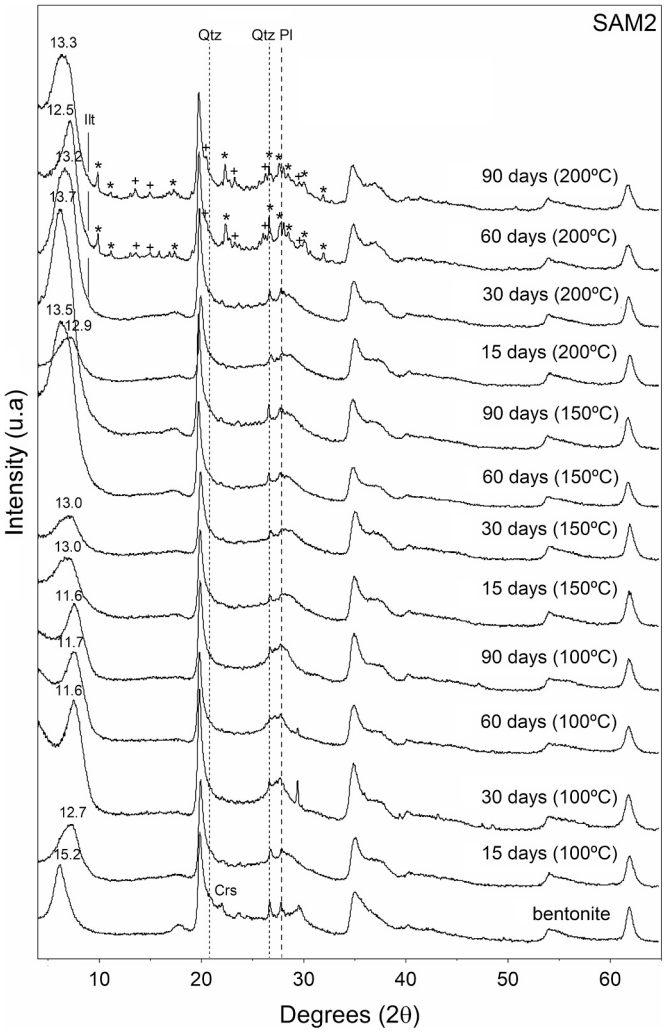

Fig. 2. XRD patterns obtained from randomly oriented mounts of starting material and solid products of reactions SAM (0.2 M) at 100, 150 and 200 °C and 15, 30, 60 and 90 days of reaction. Star: clinoptilolite, Ilt: illite, cross: buddingtonite, and Qtz: quartz.

species, alter their stability as they become more deeply-buried in the sediment column. Among these changes, minerals in the smectite group undergo structural reorganization, resulting in an increase in tetrahedral charge, the adsorption and fixation of K^+ ions in the interlayer space, and the release of silica. This leads to textural and mineralogical transformations in smectites, including the development of illitic layers and the formation of mixed-layer illite/smectite (I/S) and discrete illite. The mechanism of smectite illitization can involve multiple processes (Altaner and Ylagan, 1997), and two reaction models have been proposed: (1) A solid-state transformation characterized by layer-by-layer replacement of smectite by illite (Bethke and Altaner, 1986; Inoue et al., 1990; Amouric and Olives, 1991; Lindgreen and Hansen, 1991; Drits et al., 1997a; Cuadros and Altaner, 1998a, 1998b); or (2) Smectite dissolution followed by the crystallization of illite (Nadeau et al., 1985; Ahn and Peacor, 1986; Inoue et al., 2005; Eberl et al., 1990; Whitney and Velde, 1993; Dong et al., 1997; Murakami et al., 2005; Lanson et al., 2009; McCarty et al., 2009, Ferrage et al., 2011, Vazquez et al., 2016).

The primary source of ammonium in sedimentary basins arises from the maturation of organic matter during diagenesis, which results in transformation of complex organic compounds into simpler molecules. Specifically, protein denitrification occurs between 50 and 150 °C, releasing ammonium that can eventually be incorporated into phyllosilicates (Williams et al., 1992). Ammonium concentrations in sedimentary fluids can vary widely, from 0.54 mM in interstitial fluids in sediment within hydrocarbon basins (Bates et al., 2011) up to 150 mM in solutions from oil fields (Collins, 1975). Data collected from drilling pelagic sediments in areas of moderate to high productivity indicate very low ammonium concentration (0.001–0.03 mM) (Froelich et al., 1979), whereas interstitial water in ocean sediments in the Baltic Sea contains 1.2 mM ammonium (Carman and Rahm, 1997), or 17 mM in fluids at the Wakamiko hydrothermal field (Jo et al., 2018).

The conditions that promote transformation of smectite to illite and the simultaneous maturation of organic matter (and release of ammonium ions) can coexist in clayey sediments rich in organic matter. Authigenic phyllosilicates can absorb and fix ammonium cations (NH_4^+) into their interlayer space due to the similar ionic radius and charge as potassium (K^+) (1.43 Å NH_4^+, 1.33 Å K^+; Pironon et al., 2003). Yamamoto (1967) reported the first occurrence of ammonium in micas and Higashi (1982) referred to white micas with a predominance of ammonium as 'tobelite'. There is substantial evidence of significant NH_4^+ content in I/S and illite in sediments, both associated and not associated with hydrocarbon production basins (Williams et al., 1989; Williams and Ferrell, 1991; Drits et al., 1997b; Drits et al., 2005; Bauluz and Subias, 2010; Bobos, 2012). NH_4^+ content has also been observed in metamorphic micas (Nieto, 2002; Ruiz Cruz and Sanz de Galdeano, 2008; Bauluz and Nieto, 2018). The tetrahedral symmetry of the NH_4^+

Table 1
Estimation by FTIR of total NH_4 as interlayered cation (as % Interlayered Cations) in the altered smectite samples.

Sample	NH_4 total	NH_4 in smectite (1400 cm^{-1})	NH_4 in illite (1430 cm^{-1})
0.1 M NH_4			
100 °C			
15 days	60	53	7
30 days	79	58	21
60 days	91	72	19
90 days	99	76	23
150 °C			
15 days	22	18	4
30 days	24	21	3
60 days	39	30	9
90 days	36	28	8
200 °C			
15 days	46	33	13
30 days	70	49	21
60 days	40	28	12
90 days	43	30	13
0.2 M NH_4			
100 °C			
15 days	41	34	7
30 days	NA	–	–
60 days	NA	–	–
90 days	13	3	10
150 °C			
15 days	54	35	19
30 days	49	22	27
60 days	92	75	17
90 days	51	39	14
200 °C			
15 days	55	39	16
30 days	55	43	12
60 days	NA	–	–
90 days	64	18	48

NA: not available.

Table 2
Estimation of the percent of illite-like layers in illite/EG-smectite, derived from the difference in angular position (°Δ2θ) between 001/002 and 002/003 reflections (Moore and Reynolds, 1997). *nd*: not determined.

T (°C)	t (d)	Illite% (±3)	
		SAM1	SAM2
Untreated		0	0
100	15	*nd*	*nd*
100	30	*nd*	*nd*
100	60	*nd*	*nd*
100	90	29	*nd*
150	15	39	22
150	30	32	33
150	60	22	24
150	90	23	25
200	15	30	36
200	30	42	36
200	60	26	32
200	90	30	28

ion produces basal spacings in illite and micas that are slightly larger than those observed in the K^+ equivalents (Radoslovich, 1960).

In this study, a series of phyllosilicates were synthesized under hydrothermal conditions using a system containing bentonite with variable NH_4^+ content to investigate the influence of NH_4^+ on the smectite-to-illite transformation reaction. Samples were characterized by X-ray diffraction analysis, Fourier transformed-infrared spectroscopy and transmission electron microscopy. The results will contribute to improving our understanding of the transformation reactions that occur in phyllosilicates during diagenesis, particularly when exposed to fluids rich in ammonium and organic matter. This project seeks to test the hypothesis that fixation of NH_4^+ into smectite interlayers, contributes to stabilization of high charge layers, thus facilitating the smectite-to-illite reaction.

2. Materials and methods

Bentonite from La Serrata-Cortijo de Archidona (Cabo de Gata, Almería, SE Spain) was used as starting material. This bentonite, formed by hydrothermal alteration of volcanic tuff (Leone et al., 1983; Caballero et al., 1983, 2005), has been extensively characterized during the FEBEX project (Huertas et al., 2000). The major component of this bentonite is a Na,Ca-montmorillonite (>92%), with minor amounts of accessory minerals (quartz, feldspars, micas, calcite and amphibole) and volcanic glass. The starting material batch was prepared by grinding and homogenizing by mixing 1 kg of FEDEX bentonite, supplied by CIEMAT.

The hydrothermal treatment was studied in a chemical system that contains NH_4^+ and has a basic pH: $(NH_4)_2O$-Al_2O_3-SiO_2-H_2O (Table S1). The hydrothermal reactions were conducted in 50 cm^3 steel Teflon-lined reactors (Parr 4744), which were maintained at a constant temperature of 100, 150 or 200 °C (±3 °C) and pressure equivalent to that of corresponding water vapor pressure at different temperatures (0.101, 0.476 and 1.554 MPa), with reaction times ranging from 15 to 90 days. The bentonite powder (2 g) was mixed with 30 mL of a 0.1 or 0.2 M NH_4OH solution (Series SAM1 and SAM2, respectively); these concentrations were higher than those observed in nature to enhance the transformation of smectite to illite in a 1:15 solid:solution mass ratio. The initial pH of the solution was 11.95 (SAM1) and 11.72 (SAM2). At the end of the runs, the reactors were quenched quickly in cold water. The products were immediately centrifuged and a small fraction of the solutions was used for final pH measurement (Table S2).

The solid products of the reactions were characterized by X-ray diffraction analysis (XRD), Fourier-transform infrared spectroscopy (FT-IR) and transmission and analytical electron microscopy (TEM and AEM).

XRD analyses were performed on a PANalytical X'Pert Pro system operating at 45 kV and 40 mA with an X'Celerator detector, CuKα radiation, and a Ni filter. The goniometer (240 mm radius) was configured vertically, with a theta-theta geometry, and the sample was kept horizontal in a spinner platform. No monochromator was used. Samples were prepared in random powder and in oriented mounts. Random powders were scanned in the 2θ range from 3° to 70°, using a 0.25° divergence slit, with a 0.5° anti-scatter slit. Oriented mounts were prepared by pipetting powder dispersions in deionized water (0.1 g in 5 mL) onto glass slides, and oriented mounts were continuously scanned in the 2θ range from 3 to 40°, using a 0.125° divergence slit, with a 0.25° anti-scatter slit, in air-dried (AD), ethylene glycol-solvated (EG) and heated (sequentially, 350 °C for 1 h, then 550 °C for 2 h) states. Ethylene glycol solvation was performed within a desiccator in an oven at 60 °C for 4 h. Heating treatments were performed in a furnace at a fixed temperature.

FT-IR spectra were obtained with a PerkinElmer Spectrum One FTIR spectrometer equipped with a lithium tantalate ($LiTaO_3$) detector. Samples were prepared in KBr tablets (1% wt. sample) previously dried at 120 °C for one day. Petit et al. (1999) pointed out that NH_4^+ may be eventually replaced by K^+ form KBr in low charge layers in swelling clays, appearing as a sharp band at 1400 cm^{-1}, but NH_4^+ was not replaced by K^+ in high charge layers, which retain NH_4^+ and produced a broad band at 1430 cm^{-1}. The integrated intensity of both bands can be used for quantitative estimation of total ammonium, as well analysis of heterogeneity in layer charge and occupancy. Spectra showed differences in the intensity of the water bands, whereas the N—H bands remained unchanged. Nieto (2002) reported that NH_4^+ was stable in smectites for temperatures below 900 °C. The spectra were recorded in absorption mode and scanned with a wavenumber resolution of 4.0 cm^{-1} between 4000 and 400 cm^{-1}. A total of 100 scans were collected for each spectrum at a scan speed of 0.2 $cm{\cdot}s^{-1}$. For spectral analysis, spectra were first normalized to the O—H stretching band at ~3630

Table 3
Representative analyses of untreated bentonite (average of several analyses; *sd*, standard deviation) and synthetic samples SAM1 formed at 100, 150 and 200 °C after 90 days, normalized to $O_{10}(OH)_2$.

	Si	Al^{IV}	Al^{VI}	Fe^{3+}	Mg^{VI}	Na	K	Ca	Mg	
Untreated ($n = 5$)	3.85	0.15	1.44	0.20	0.37	0.18	0.06	0.09	0.16	
sd	*0.08*	*0.08*	*0.04*	*0.07*	*0.08*	*0.06*	*0.05*	*0.01*	*0.05*	
Ref.	Si	Al^{IV}	Al^{VI}	Fe^{3+}	Mg^{VI}	Na	K	Ca	NH_4	
100 °C 90 d										
10C	3.94	0.06	1.49	0.10	0.41	0.00	0.00	0.12	0.23	S
15C	3.90	0.10	1.53	0.03	0.44	0.00	0.03	0.08	0.33	S
16C	4.00	0.00	1.45	0.22	0.33	0.00	0.05	0.16	0.00	S
17C	3.83	0.17	1.60	0.09	0.31	0.00	0.29	0.00	0.19	S
20C	3.92	0.08	1.45	0.15	0.40	0.00	0.02	0.19	0.08	S
21C	3.86	0.14	1.38	0.19	0.43	0.00	0.02	0.24	0.07	S
1C	3.54	0.46	1.13	0.31	0.56	0.00	0.10	0.19	0.55	I/S
2C	3.62	0.38	1.25	0.14	0.61	0.00	0.03	0.22	0.52	I/S
3C	3.67	0.33	1.14	0.15	0.71	0.00	0.03	0.20	0.60	I/S
4C	3.62	0.38	1.15	0.20	0.64	0.00	0.03	0.20	0.59	I/S
5C	3.70	0.30	1.23	0.24	0.53	0.00	0.00	0.22	0.39	I/S
6C	3.75	0.25	1.30	0.20	0.49	0.00	0.02	0.19	0.35	I/S
7C	3.76	0.24	1.41	0.08	0.51	0.00	0.02	0.17	0.40	I/S
8C	3.67	0.33	1.27	0.17	0.56	0.00	0.02	0.17	0.54	I/S
9C	3.77	0.23	1.27	0.10	0.63	0.00	0.03	0.20	0.42	I/S
11C	3.66	0.34	1.31	0.14	0.55	0.00	0.02	0.34	0.19	I/S
12C	3.73	0.27	1.10	0.27	0.63	0.00	0.05	0.20	0.44	I/S
13C	3.66	0.34	1.31	0.14	0.55	0.00	0.02	0.34	0.19	I/S
14C	3.76	0.24	1.35	0.17	0.48	0.00	0.03	0.17	0.35	I/S
18C	3.71	0.29	1.05	0.32	0.63	0.00	0.10	0.12	0.58	I/S
19C	3.53	0.47	1.15	0.35	0.50	0.00	0.00	0.10	0.77	I/S
average in S	3.91	0.09	1.48	0.13	0.39	0.00	0.07	0.13	0.14	
average in I/S	3.68	0.32	1.23	0.20	0.57	0.00	0.03	0.20	0.46	
150 °C 90 d										
3B	3.84	0.16	1.32	0.14	0.55	0.00	0.00	0.20	0.30	S
5B	3.83	0.17	1.31	0.12	0.57	0.00	0.02	0.28	0.17	S
8B	3.90	0.10	1.47	0.07	0.46	0.00	0.03	0.19	0.15	S
11B	3.94	0.06	1.42	0.14	0.45	0.00	0.02	0.19	0.11	S
12B	3.80	0.20	1.60	0.10	0.30	0.00	0.02	0.08	0.33	S
13B	3.82	0.18	1.58	0.10	0.32	0.00	0.00	0.12	0.26	S
14B	4.00	0.00	1.36	0.19	0.46	0.00	0.00	0.08	0.29	S
15B	3.83	0.17	1.28	0.08	0.64	0.00	0.02	0.07	0.66	S
16B	3.80	0.20	1.44	0.15	0.41	0.00	0.00	0.12	0.37	S
1kB	3.56	0.44	1.22	0.14	0.64	0.00	0.05	0.22	0.59	I/S
2B	3.73	0.27	1.25	0.15	0.60	0.00	0.03	0.20	0.42	I/S
4kB	3.61	0.39	1.14	0.12	0.74	0.00	0.03	0.20	0.70	I/S
6B	3.50	0.50	1.36	0.19	0.46	0.00	0.03	0.17	0.59	I/S
7B	3.70	0.30	1.12	0.25	0.63	0.00	0.08	0.14	0.57	I/S
9B	3.76	0.24	1.21	0.40	0.40	0.00	0.12	0.19	0.14	I/S
10kB	3.72	0.28	1.46	0.15	0.39	0.00	0.00	0.17	0.33	I/S
17B	3.73	0.27	1.22	0.19	0.59	0.00	0.02	0.15	0.54	I/S
average in S	3.86	0.14	1.42	0.12	0.46	0.00	0.01	0.15	0.29	
average in I/S	3.66	0.34	1.25	0.20	0.56	0.00	0.05	0.18	0.48	
200 °C 90 d										
4A	3.92	0.08	1.20	0.17	0.64	0.00	0.12	0.21	0.17	S
5A	3.96	0.04	1.31	0.12	0.57	0.00	0.07	0.21	0.55	S
6kA	3.99	0.01	1.41	0.12	0.47	0.00	0.08	0.20	0.39	S
8A	3.78	0.22	1.15	0.34	0.51	0.00	0.27	0.21	0.45	S
9 A	4.00	0.00	1.26	0.22	0.52	0.00	0.03	0.20	0.49	S
12 A	3.85	0.15	0.96	0.42	0.62	0.00	0.45	0.22	0.32	S
1 A	3.62	0.38	1.18	0.23	0.59	0.00	0.15	0.23	0.82	I/S
2 A	3.50	0.50	1.03	0.25	0.72	0.00	0.18	0.25	1.03	I/S
10kA	3.75	0.25	1.26	0.18	0.55	0.00	0.15	0.22	0.66	I/S
average in S	3.92	0.08	1.21	0.23	0.56	0.00	0.17	0.21	0.40	
average in I/S	3.62	0.38	1.16	0.22	0.62	0.00	0.16	0.23	0.83	

S: smectite-type particles; I/S: illite/smectite-type particles.

cm^{-1} (Higashi, 2000; Petit et al., 2006). Subsequently, the NH_4^+ deformation band was decomposed using least-squares fitting with Gaussian shape functions to estimate the integral intensity of the total band and of each component.

In addition to the treated samples, a set of NH_4^+-montmorillonite samples from 0% to 100% in NH_4^+ was prepared. Ammonium and potassium homoionic smectites were prepared by suspension of raw bentonite in 0.1 M NH_4Cl and 0.1 M KCl solutions, respectively. The resulting NH_4^+ and K^+ saturated smectites were mixed by grinding in appropriate proportions. Their FT-IR spectra revealed a single maximum

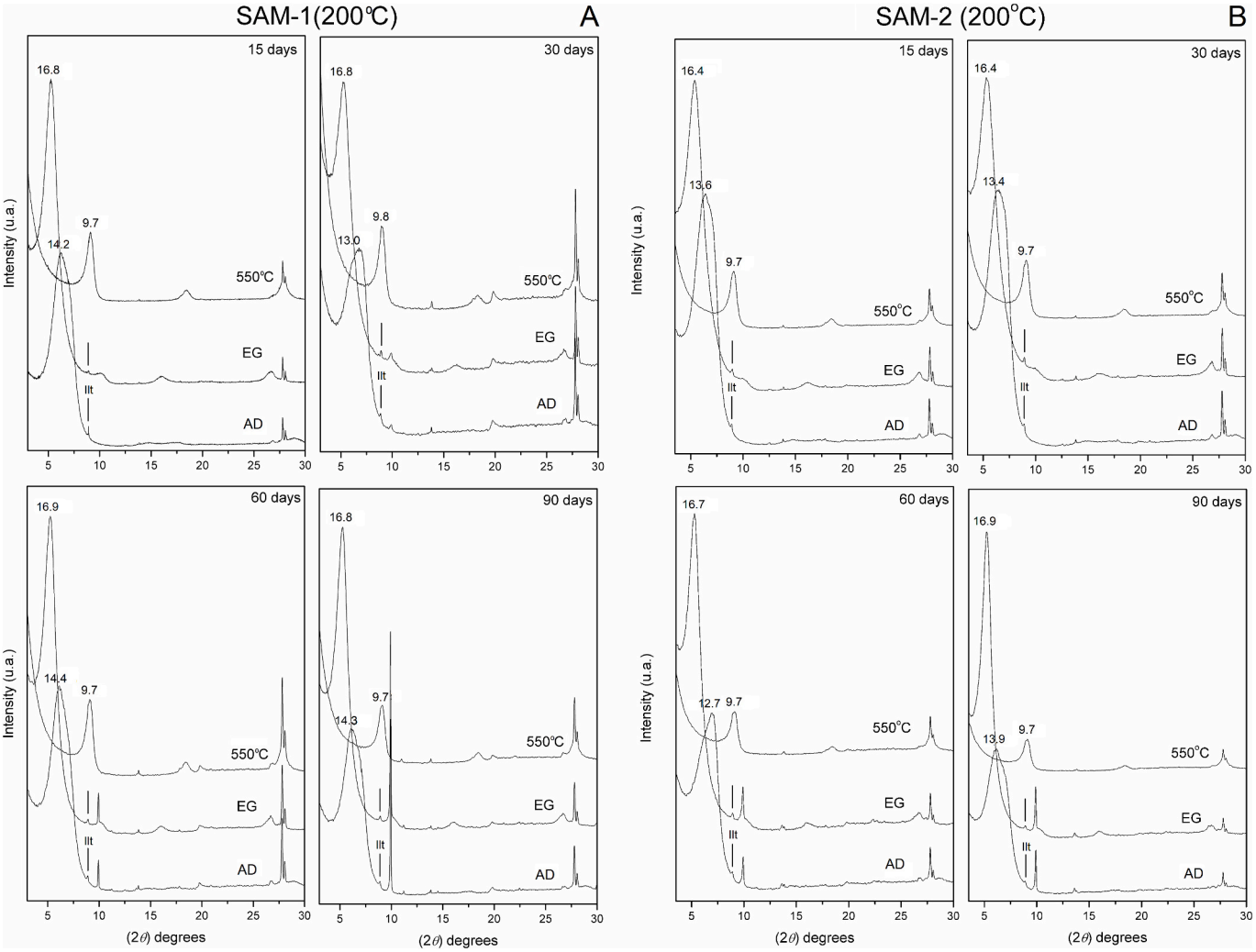

Fig. 3. XRD patterns from oriented samples: (A) SAM (0.1 M and 200 °C; (B) SAM (0.2 M and 200 °C). AD: oriented airdried, EG: ethylene-glycol treatment, and 550 °C: heated at 550 °C.

at 1400 cm^{-1}, whose integral intensity linearly correlated with the NH_4^+ content in the interlayer space. This relationship was used to estimate the ammonium content in the treated samples (estimated error < 20%).

The mineralogical compositions, crystal chemistry, and texture (i.e., arrangement, size, shape, and spatial configuration of particles) of solid reaction products were analyzed using two microscopes. A Philips CM-20 microscope (CIC, University of Granada) fitted with an ultrathin window, with a LaB6 filament, operated at 200 kV, and point-to-point resolution of 2.7 Å was used for TEM and AEM, with the aim of obtaining quantitative analyses of individual particles. Chemical analysis was collected in STEM (scanning transmission electron microscopy) mode, using a bright field detector, with an EDAX © solid-state Si(Li) detector for energy dispersive X-ray (EDX) analysis. Scan window ranged from 50 × 100 to 200 × 200 Å. Atomic % was calculated by the thin film ratio criteria, following the procedure of Cliff and Lorimer (1975) and Champness et al. (1981). A variety of natural mineral standards (e.g., albite, biotite, spessartine, muscovite, forsterite, annite and titanite) were used to obtain K-factors to transform intensity ratios to concentration ratios. The second microscope used for high-resolution TEM (HRTEM) was a JEOL-2000 FXII instrument (SAI, University of Zaragoza) operated at 200 kV, equipped with an Oxford 200X-Sight Instruments detector. The <2 μm fraction of each specimen were prepared in two modes: encased within an epoxy resin and sliced parallel to the c-axis, and dried from ethanol suspension on Cu grids. TEM images and AEM analyses were obtained with CM-20 in Cu-grids, while HRTEM analysis was done with a JEOL-2000 FXII in ultrathin sections. Chemical analyses obtained at nano-scale by AEM were converted to structural formulae. In the untreated bentonite, the formulae were calculated on the basis of $O_{10}(OH)_2$ assuming 22 negative charges, since all cations were analyzed. An octahedral occupancy apparently higher than 2 is due to a fraction of Mg^{2+} ions located in the interlayer space, according to the exchangeable cation analysis in bulk sample (Huertas et al., 1995). The structural formulae of treated samples were computed on the basis of $O_{10}(OH)_2$, and assuming that the tetrahedral plus octahedral occupancy is 6 atoms per formula unit (apfu) (Nieto, 2002). The NH_4 content could not be measured by AEM and thus was estimated as the difference required to satisfy interlayer charge.

3. Results

The combined results from XRD, FTIR and TEM, reveal significant mineralogical, crystal-chemical and textural changes resulting from the hydrothermal treatment of bentonite. These changes are attributed to smectite alteration and transformation reactions leading to the formation of new phases. The chemistry and mineralogy of the synthesized samples depend on the composition of the treating solution (i.e., NH_4^+ concentration), temperature, and reaction time. Notably, the pH of the hydrothermal solution decreased rapidly from its initial value of approximately 12 to 11 after 15 days of hydrothermal treatment, followed by a slower decline to ~10 (SAM1) and ~ 9 (SAM2) after 90 days.

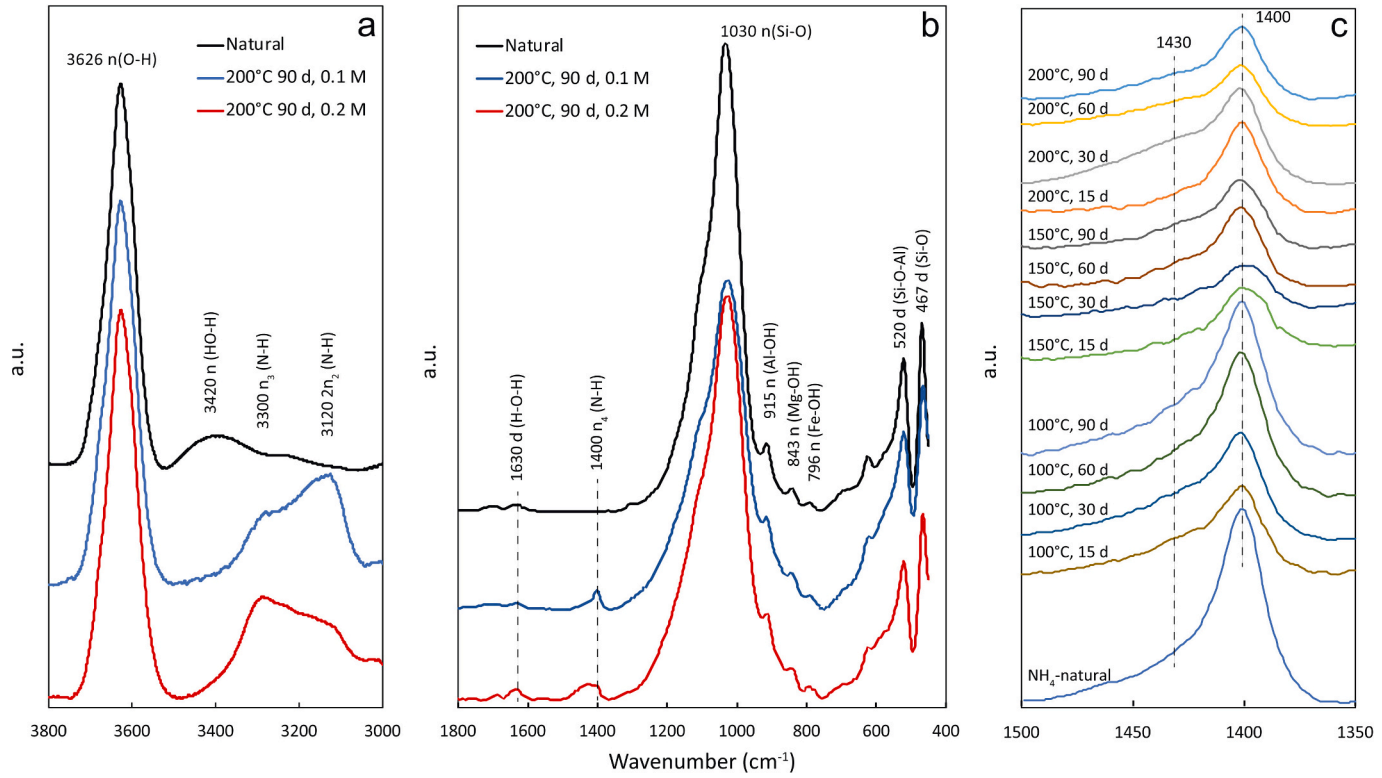

Fig. 4. FTIR absorption spectra of samples SAM1 and SAM2 (200 °C, 90 days of reaction) and untreated smectite: (A) high wavenumber (3800–3000 cm^{-1}) and (B) low wavenumber (1800–450 cm^{-1}) spectral regions. (C) δ^{+}_{NH4} deformation vibration modes (ν_4) band of SAM1 samples and the untreated smectite saturated with ammonium (NH_4-natural).

3.1. X-ray diffraction analysis

The XRD patterns obtained from the randomly oriented solid products of reactions conducted with two different ammonium concentrations (0.1 and 0.2 M), at different temperatures (100, 150 and 200 °C), and for different reaction times (15, 30, 60, and 90 days), together with the pattern of the starting smectite, revealed that the smectite 001 basal spacing decreased from 15.2 Å in the untreated sample to 12.6–13.5 Å (0.1 M, Fig. 1) and to 11.6–13.7 Å (0.2 M, Fig. 2). This reduction in basal spacing was more pronounced when increasing the NH_4^+ concentration from 0.1 to 0.2 M. This behavior was interpreted as resulting from the incorporation of NH_4^+ ions from solution into the interlayer space, leading to the partial release of the natural cations Ca^{2+} and Na^+. NH_4^+ ion behavior within the interlayer space differs from cations such as Na^+, K^+, or Ca^{2+}, due to its ionic radius and hydration energy. The basal spacing of NH_4 montmorillonite remained at around 12.0 Å for a wide range of relative humidity (20–70%), which corresponds to a monolayer of water molecules (Gautier et al., 2010; Wakakita et al., 2023). Furthermore, NH_4^+ ions can form multiple hydrogen bonds with oxygen atoms in the basal tetrahedral sheet, further limiting the swelling of the interlayer spacing during hydration (Díaz Pinthier, 1999). The difference in ionic radii between NH_4^+ and K^+ also enlarged the basal spacing of ammonium illite to 10.3 Å, compared with 10.0 Å for the K^+ end-member (Drits et al., 1997a, 1997b). A small reflection at ~10 Å suggests the partial transformation of the untreated smectite into packets or crystals of discrete illite. This reflection was observed in powder patterns in the experiments conducted at 150 and 200 °C after 15 days of reaction with 0.1 M NH_4^+, and after 30 days at 200 °C with 0.2 M NH_4^+. In other conditions, this reflection could be hidden within the broad basal reflection of smectite. The formation of non-swelling layers within the smectite crystals produced disordered I/S regions, contributing to a reduction in the basal spacing of the reacted samples.

Octahedral sheet composition in phyllosilicates influences the *b* parameter which is typically derived from the (060) reflection included within the (06*l*, 33*l*) band at 1.54–1.49 Å (see the recent review of Petit et al., 2023). The spacing of the (06*l*, 33*l*) reflections was measured in powder diffractograms using quartz as an internal standard (Fig. S1). The value of *b* was quantified as 6 times $d_{(06l,33l)}$ (Fig. S2), obtaining 8.992 Å for the untreated montmorillonite. In the case of SAM1, almost no variation was observed in *b*, with values occurring within 0.010 Å. SAM2 samples exhibited a slight increase of the $d_{(06l,33l)}$ with time, which indicated that the higher ammonium concentration induced some changes in the octahedral layer composition. The data available did not allow us to derive either a statistically significant trend with time or a correlation with temperature.

Quartz was identified in the untreated bentonite, as well as in all the samples, although the intensity of the main reflection (the 101 peak at 3.34 Å) varies with treatment (Figs. 1 and 2). The intensity of reflections decreases with time at 100 °C, while at 200 °C, the intensity is initially very low but increases with treatment time. This behavior is attributed to quartz dissolution (100 °C) and precipitation or recrystallization (200 °C). Furthermore, clinoptilolite (a zeolite) and buddingtonite (NH_4^+feldspar) were identified in samples treated at 150–200 °C for a longer time. Comparing both series, the precipitation of byproducts was more relevant in SAM2 than in SAM1. According to these results, dissolution and byproduct precipitation become more pronounced with increasing temperature and ammonium concentrations. Precipitation of NH_4-bearing phases may scavenge NH_4^+ from solution.

Diffraction patterns of the oriented mounts are consistent with the observations in random powder patterns. Samples obtained at 100 °C (Fig. S3) exhibited an asymmetric 001 basal reflection at 12.3–13.6 Å (0.1 M) and 12.2–12.3 Å (0.2 M) in AD mounts, which partially expanded to 12.7–16.4 Å (0.1 M) and 12.9–15.2 Å (0.2 M) in EG, to finally collapse to ~10 Å after heating at 550 °C. At 150 and 200 °C (Figs. S4 and 3), both series of samples exhibited similar behavior. The basal reflections at 13.0–14.5 Å (0.1 M) and 12.4–13.9 Å (0.2 M) in the

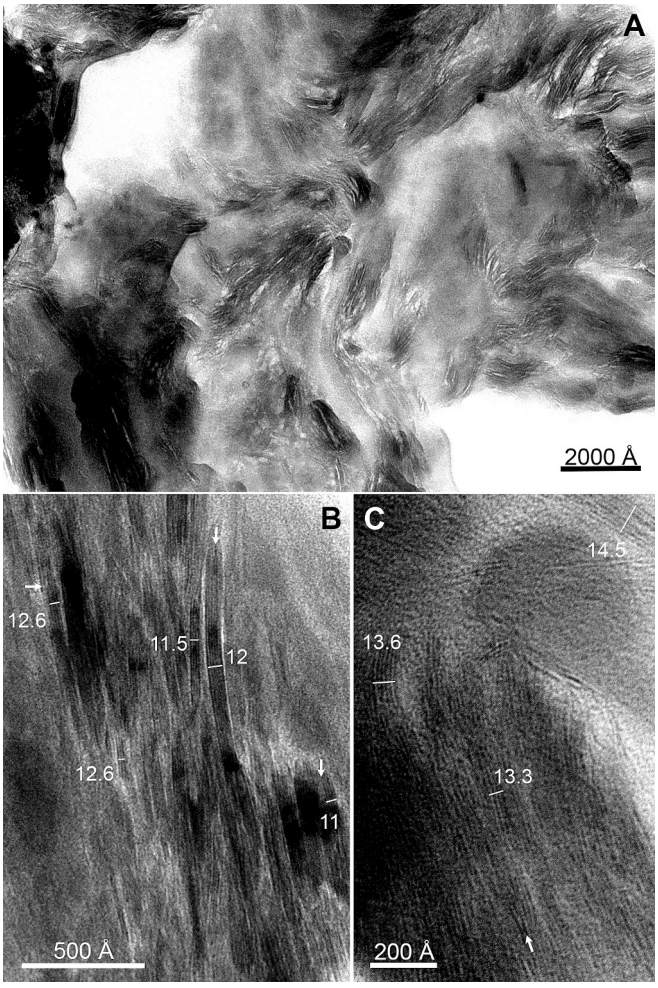

Fig. 5. TEM images of untreated bentonite. (A) Low magnification image showing the curved smectite flakes of irregular outline. (B) Single smectite particles are stacks of a few layers, usually <10 layers; with periodicities in the range of 11 to 15 Å, and abundant defects and lateral layer terminations or splitting (see arrows). (C) Detailed texture of curved smectite particles with spacings between 13.3 and 14.5 Å, with wedge terminations (arrow).

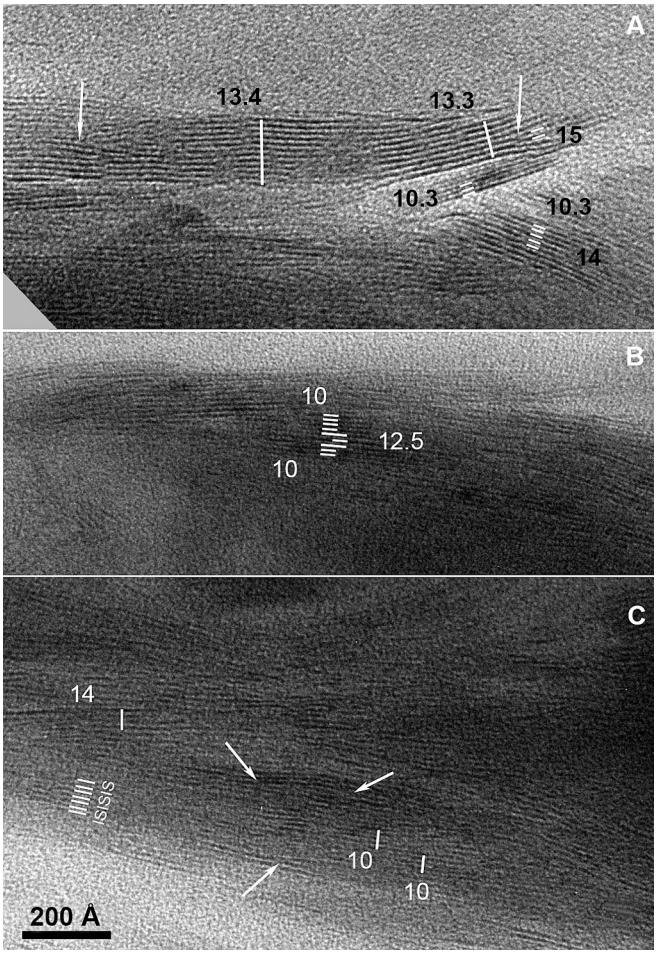

Fig. 6. High magnification images of particles in sample SAM1C treated at 100 °C for 90 days that showed different basal spacing, and layer ordering. (A) A crystal of smectite with abundant defects (arrows) and layer spacing of 13.3 Å, that expand to 15 Å on the right end by layer splitting. A planar crystal with spacing of 10.3 Å may correspond to illite layers with interlayered ammonium. Smectite and illite layers coexist in same particles. (B) A particle composed of thin stacks of several layers with periodicities of 10 and 12.5 Å that may correspond to disordered I/S particles. (C) A particle of about 50 nm in thickness that contains smectitic (14 Å) and illitic (10 Å) domains, as well as an ordered sequence of I/S layers. Arrows denote along-layer terminations that represent the smectite to illite reaction fronts.

AD series swelled to 16.6–16.9 Å (0.1 M) and 16.4–16.9 Å (0.2 M) in the EG series, approaching the characteristic 17 Å spacing of pure smectite layers. Upon heating at 550 °C, the samples collapsed to ~10 Å.

The existence of a disordered I/S phase rich in smectite was supported by a basal spacing (001) <17 Å, no rational series of (00*l*) reflections in EG, and the disappearance of the (003) reflection after heating at 350 °C for 1 h. An estimation of the percent of illite-like layers in mixed-layer illite/EG-smectite can be derived from the difference in angular position (°Δ2θ) between 001/002 and 002/003 reflections (Moore and Reynolds, 1997). The results are gathered in Table 2. The results varied between 20 and 40% of illite layers. A very rough trend indicates that a higher proportion of illite corresponds to 15 d samples and that % illite layers decrease with reaction time up to 90 d. Temperature and ammonium concentration contributed to forming I/S with higher illite content. In samples synthesized at 100 °C these higher order reflections were very weak, likely due to high smectite content, and no estimate of precise % smectite layers could be obtained.

A diffraction peak at ~10 Å was more easily observed in oriented mounts than in powder patterns. No individual 10 Å reflections was observed at 100 °C, but a small shoulder on the 001 smectite reflection occurred in both AD and EG mounts. At 150 and 200 °C it was a small, sharp reflection that did not shift position after EG treatment. This behavior suggests the existence of a small fraction of discrete illite crystals.

3.2. FT-IR spectroscopy

The IR spectra of the samples displayed the characteristic bands of montmorillonite with no relevant differences observed in the structure bands compared with the raw bentonite or between different samples, irrespective of reaction time, temperature or ammonium concentration (Fig. 4). Specifically, the broad band near 3420 cm^{-1} and the band at 1637 cm^{-1} correspond to OH stretching vibration and bending vibration of absorbed water, respectively. The band at 3626 cm^{-1} was assigned to the stretching vibration of OH groups within the octahedral sheet (Fig. 4A). In the low wavenumber region, the strong band at 1031 cm^{-1}, indicative of Si—O stretching vibrations, is associated with fourfold-coordinated silica. The bands at 915, 843 and 796 cm^{-1} correspond to M-OH bending linked to various octahedral cations (Al^{3+}, Fe^{3+}, Mg^{2+}; Farmer, 1974). Additionally, the bands at 519 and 467 cm^{-1} are attributed to Si-O-Al and Si-O-Si bending vibrations (Farmer, 1974) (Fig. 4B).

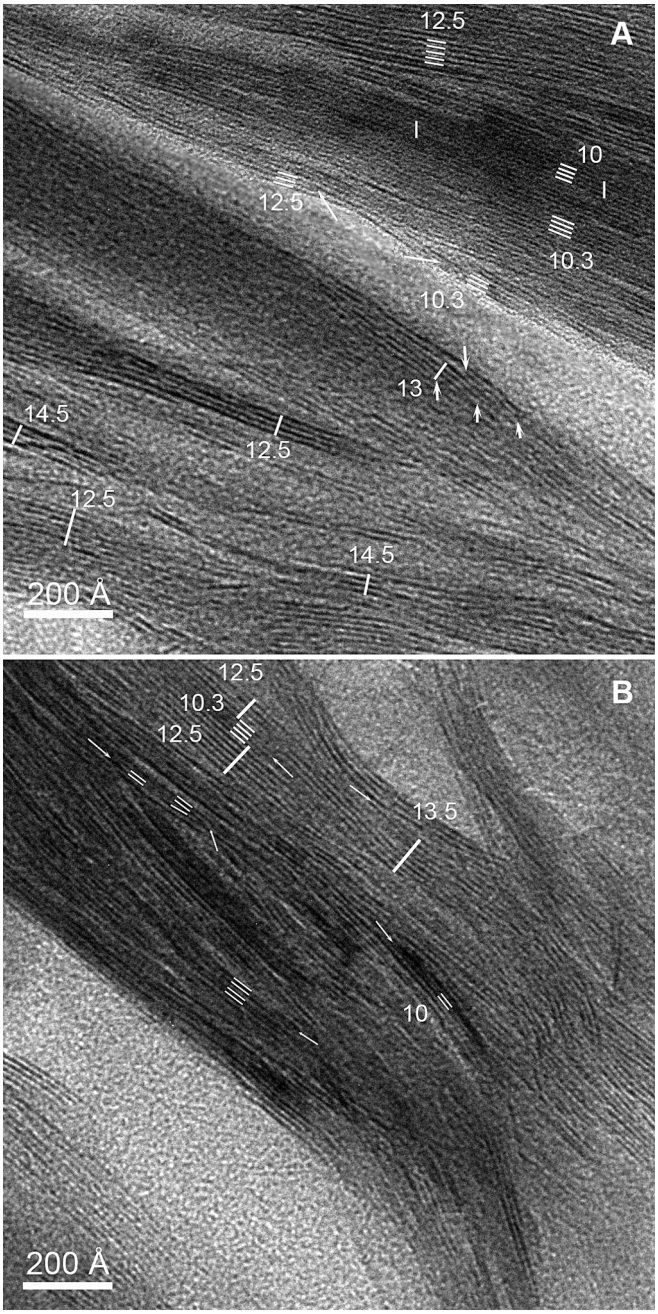

Fig. 7. High magnification images of particles in sample SAM1B treated at 150 °C for 90 days. (B) Packet of smectite crystals (bottom) with spacing that varied from 12.5 to 14.5 Å; thinner crystals showed a more wavy shape than thicker ones (top). Arrows denoted layer termination defects. Also shown (middle) is a 30–40 nm thick illite crystal (I) composed of layers with basal spacing of 10 and 10.3 Å. Note the contrasting texture of illite (planar) and smectite (wavy). The outer side showed smectite layers (12.5 Å) and illite layers (10.3) connected by a less crystalline transition region with lateral layer terminations (long arrows). (D) Packet of smectite crystals with intercalation of illite layers (1–3) (parallel marks), associated to along layer termination defects (arrows), that are interpreted to correspond to smectite-to-illite reaction fronts.

The FT-IR spectra confirmed the presence of NH_4^+ absorbed on smectites. Notably, a small band with the range of 1400–1430 cm^{-1} corresponds to δ_{NH4}^+ deformation vibration modes (ν_4). Four poorly-defined bands were assigned to: the $\nu_{N\text{-}H}$ stretching vibrations at 3300 cm^{-1} (ν_3), the overtone 3119 cm^{-1} ($2\nu_2$), and the combination vibration 2927 cm^{-1} ($\nu_2 + \nu_4$). Additionally, a band at 2851 cm^{-1} ($2\nu_4$) represents the first harmonic of the deformation vibration (Shigorova et al., 1981; Petit et al., 1998, 2006; Harlov et al., 2001).

In some samples, the deformation vibration band exhibited a main peak at ~1400 cm^{-1}, along with a shoulder or a smaller band at ~1430 cm^{-1} (Fig. 4C). The relative intensity of these features varied among samples, as previously observed by Šucha et al. (1998). The total integral intensity of the 1400–1430 cm^{-1} band can be used to estimate the total NH_4^+ content within smectites. Specifically, the 1400 cm^{-1} band corresponds to exchangeable NH_4^+ in low charge layers, whereas the 1430 cm^{-1} shoulder represents NH_4^+ in high charge layers (Petit et al., 1998).

The integral intensity of the 1400–1430 cm^{-1} band provided an estimate of the total ammonium content, while the integral intensity of 1400 cm^{-1} band corresponded to NH_4^+ in the smectite layers. The difference between these values represents an estimation of NH_4^+ in illite-type layers (Table 1). The results obtained show that, on average, the ammonium content accounted for 50% of the interlayer cations, with a wide range of variation depending on temperature and aging time. On the other hand, the amount of ammonium adsorbed on smectite layers is higher than the ammonium fixed in illite-like layers. This observation is consistent with XRD results that indicate a prevalence of smectite layers after the hydrothermal treatment.

3.3. Transmission and analytical electron microscopy

A subset of samples was selected for HRTEM and AEM observations in order to detect changes in particle morphology and lattice fringes resulting from the illitization reaction. Additionally, chemical microanalysis was performed on individual particles using Cu-grid mounted samples. The increase in interlayer K^+ or NH_4^+ and tetrahedral Al content served as an indicator of the progress of illitization.

The untreated smectite exhibits irregular and undulating flakes and stacks of curved particles with laminations typically around 50 nm in thickness, which is characteristic of smectite (Fig. 5A). Close examination of lattice-fringe images of smectite (Fig. 5B) revealed stacks of particles (~100 × 15 nm) with spacings between 11 Å and 15 Å (most commonly 12–12.2 Å). Individual smectite particles appeared as curved flakes with a wavy appearance and showed numerous edge dislocations and terminations of smectite layers (arrows, Fig. 5B,C).

The solid products of the SAM1 reaction at 100, 150, and 200 °C, after 90 days, were selected for HRTEM and AEM analysis. The study of these samples revealed some differences compared to the raw material. The particles were slightly less curved, had well-defined outlines, and locally thicker stacks of platy particles (typically 50 nm thick, reaching up to 120 nm at 200 °C). Occasionally, polygonal particles corresponding to K- or NH_4-feldspars and zeolites, which were byproducts of smectite dissolution, were observed. The basal lattice-fringe images revealed defects in layer stacking, including lateral and wedge terminations, layer splitting, and deformation (bending of several layers). This texture of along-layer terminations and defects corresponds to the smectite-to-illite reaction front.

The 100 °C sample consists of subparallel crystals with low-angle contacts exhibiting partial curvature and bending, and with a thickness on the order of several nanometers, occasionally reaching up to 35 nm. This mixture included smectite, I/S and illite (Fig. 6). Stacks of platy particles displayed lattice fringes with spacings of 12.5, 13.5 and 15 Å. In some regions, layers with spacings between 12 and 15 Å coexisted, likely corresponding to smectite crystals of varied expandability (Fig. 6A). Within the smectite domains, single layers with a 10 Å spacing were frequently identified. Occasionally, crystals with basal spacing of 10.3 Å were observed and interpreted as illite layers with interlayer ammonium (Fig. 6A). Assuming that a 10 Å spacing corresponds to illite and 12–15 Å spacings to smectite layers, crystals of I/S were also observed with irregularly ordered spacings at 10 Å and 12–15 Å (Fig. 6B). These randomly interstratified I/S particles varied in thickness and length. Additionally, small domains of ordered I/S sequences were present, including IISS, ISSI, and even ordered I/S layers with a spacing of 24 Å, consisting of 2, 4 or 6 layers (Fig. 6C). Occasionally, packs of

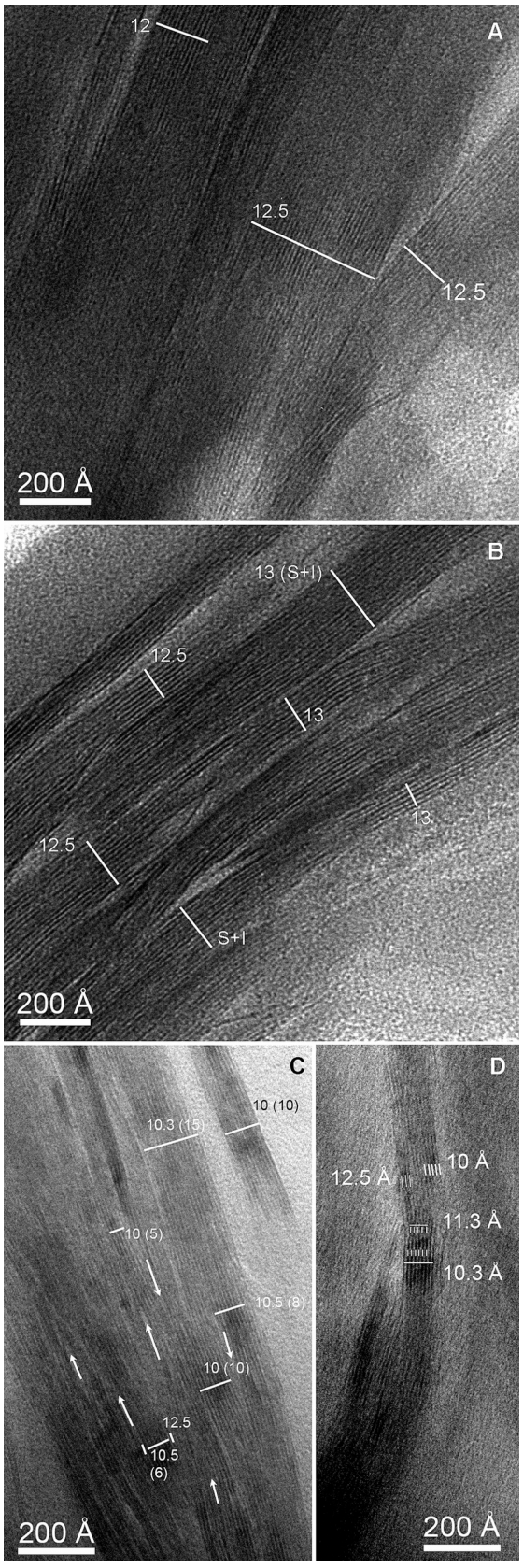

(caption on next column)

Fig. 8. High magnification images of particles in sample SAM1 A tread at 200 °C for 90 days. (A) A thick smectite particle (>100 nm) consisting of several planar smectite crystals with regular spacing of 12.5 Å, connected by low angle contacts. (B) Crystals consisting of disordered I + S layers, preserving bending, wedges and layer splitting. (C) Stack of illite crystals (5 to 15 layers) with basal spacing between 10 and 10.5 Å, including single layer of smectite (12.5 Å). Crystals exhibited low angle contact as well as frequent layer splitting (arrows) and wedges. (D) A thin crystal composed of illite and smectite layers. From top to bottom, basal spacing changed from 12.5 Å to 11.3 Å, and finally to 10.3 Å, following an along-layer transformation of a smectite-to-illite reaction.

regular spaced 10 Å layers were observed, reaching up to 5 nm in thickness (Fig. 6C).

After reaction at 150 °C, particles were thicker compared to those at 100 °C, with thickness reaching 80–100 nm. These particles typically measured 10–25 nm in thickness and were composed of parallel or subparallel crystals exhibiting less waviness than those obtained at 100 °C. Most crystals displayed regular spacing, predominantly at 12.2–12.5 Å, although spacings of 13–15 Å were also common (Fig. 7A). Smectite domains typically consisted of stacks containing 5 to 10 layers. Frequent defects and lateral layer discontinuities led to lateral and wedge terminations due to layer disappearance or splitting. Smectite crystals consisting of 2–3 layers were also observed, with spacing that varied between 12 and 15 Å, and having a curved shape (Fig. 7B). Illite layers with spacings of either 10 or 10.3 Å usually appeared inter-stratified within the smectite crystals, either as single layers or as stacks of 2–4 layers thick, occasionally associated to along-layer terminations (Fig. 7B). Domains of I/S were also observed, such as those with a 10 + 12.5 Å spacing (i.e. adjacent 10 and 12.5 Å layers). While crystals composed almost exclusively of illite layers were rarely observed, they do occasionally reach thicknesses of tens of nanometers and include layers of both 10 and 10.3 Å thickness, as well as smectite layers at the outer sides (Fig. 7A).

The samples obtained after reaction at 200 °C contained thicker particles compared to those produced at lower temperature, often exceeding 100 nm in thickness. These particles were frequently composed of planar crystals consisting of 20–40 smectite layers with regular spacing, usually around 12–12.5 Å. These smectite crystals showed low-angle contacts, layer continuity spanning over 100 nm, and common layer splitting defects (Fig. 8A). Thin crystals with <5 smectite layers were also observed, often exhibiting defects. Occasionally, 10 Å layers were interspersed within the smectite crystals, similar to what was observed at lower temperatures. Thinner smectite crystals showed bending defects and could contain domains of I/S layers, ranging from disordered (Fig. 8B) to occasionally ordered (e.g., SISI). Discrete illite crystals, more common at 200 °C than at lower temperatures, exhibited planar morphology and lattice fringes measuring 10–10.3 Å. They were usually aggregated in particles showing low-angle contact or stacked through a less crystalline band in between (Fig. 8C). Bending in these crystals may be associated with previously transformed smectite crystals (Fig. 8C). Some crystals displayed reaction fronts of the smectite-to-illite transformation, evident as along-layer transformations where spacings decrease from ~12.5 to 10 Å (Fig. 8D). Layers with spacings <10 Å were occasionally observed within these reaction fronts and may indicate areas undergoing transformation through rearrangement.

The chemical composition of the particles corresponds to both smectitic and illitic phases (Table 3). The analyses of smectite crystals in the untreated bentonite, based on $O_{10}(OH)_2$ calculation, indicates that a fraction of the Mg^{2+} ions are located in the interlayer space, consistent with exchangeable cation analysis of the bulk sample (Huertas et al., 1995). The occurrence of octahedral Mg^{2+} and low tetrahedral Al^{3+} classify the smectite as a montmorillonite (average $Si_{3.85}$). The analyses of altered samples showed that the chemical composition of the stacks of curved particles was similar to that the composition of particles of the untreated smectite, with Si contents in the range 3.78 to 3.96 apfu. The cation exchange reactions induced by the treatment with NH_4^+ solutions

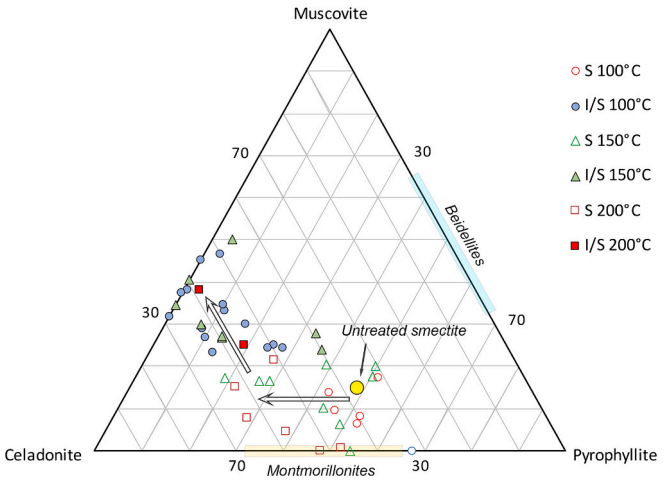

Fig. 9. Representation of the chemical composition of particles analyzed by AEM in STEM-mode in a ternary Muscovite-Pyrophyllite-Celadonite diagram. The data have been derived from Table 3. Open symbols correspond to smectite and solid symbols stand for I/S particles.

caused the presence of NH_4^+ as interlayer cation. Since NH_4^+ could not be analyzed by AEM in the CM20 microscope, a sample was prepared by sedimentation on a Cu-grid and observed using a FEI Titan G2 60–300 microscope (CIC, University of Granada) to confirm the presence of NH_4^+ ions. EDX spectra of several particles revealed a peak corresponding to N, which disappeared after a few seconds due to N volatilization under the beam energy. The analysis of thin particles showed lower Si content (3.50–3.70 apfu), and higher Al^{IV} (>0.30) and Mg^{VI} (>0.5) contents (Table 3). Additionally, these particles showed a higher layer charge, consistent with the presence of some illitic layers.

Direct comparisons between the textural (HRTEM, ultrathin sections) and chemical (AEM, Cu grids) analyses are not straightforward. HRTEM observations reveal that most illite layers are included within particles that also contain stacks of smectite layers. However, the AEM analyses were performed on single particles sedimented on Cu grids and, consequently, the analyses frequently corresponded to particles containing smectite, illite and/or I/S domains. To differentiate between smectite-rich particles and those containing illite or I/S crystals, a value of Si = 3.74 apfu was adopted as a reasonable threshold. This value is close to the 4 apfu for a pure montmorillonite.

4. Discussion

Many studies of smectite illitization have conducted experimental reactions to better understand the controlling parameters of this transformation (e.g., Eberl, 1978; Roberson and Lahann, 1981; Inoue, 1983; Huang et al., 1986; Huang, 1993; Cuadros and Linares, 1996; Mosser-Ruck et al., 1999, 2001; Dong, 2005; Ferrage et al., 2011; Fang et al., 2017). They have concluded that illitization is favored by temperatures in the range of 100 to 250 °C, high liquid/solid ratio, high pressure, a dioctahedral nature of smectite, a stoichiometric amount of K, and the presence of water or chloride solution.

In the synthesis experiments described in this work, XRD patterns revealed that smectite incorporates NH_4^+ into its structure, resulting in an asymmetric reflection at 11.5–14.5 Å, which may correspond to two overlapping reflections: one at ~15 Å associated with smectite with two water layers, and another at ~12 Å for smectite with one water layer, characteristic of NH_4-smectite (Gautier et al., 2010; Wakakita et al., 2023). SAM2 samples (0.2 M NH_4) exhibited a lower spacing than SAM1 (0.1 M NH_4) likely due to a higher proportion of layers intercalated with ammonium in SAM2 samples. Some smectite particles, containing layers transformed into illite, expanded to <17 Å in ethylene-glycol vapor (Figs. S3, S4, 3). The 001 basal spacing in EG expanded to 16.6–16.9 Å at 150 and 200 °C and to a wider range (12.7–16.4 Å) at 100 °C. The analysis of the EG patterns showed that illite layers were interstratified with the smectite layers, forming a disordered I/S with 20–40% illite layers. Increasing temperature and ammonium concentration enhanced the illite content, but increasing time decreased illite % in mixed-layer I/S. This last effect of time could be associated with the formation of discrete illite at the expense of I/S.

The formation of discrete illite was evident from the appearance of a small XRD peak at approximately 10 Å, one that is more clearly observed in oriented mounts than in powder patterns, as a small shoulder at 100 °C (Fig. S3) and discrete peak at 150° (Fig. S4) and 200 °C (Fig. 3). Qualitatively, it can be said that time, temperature and ammonium favor the formation of illite.

According to XRD results, the smectite transformed into a mixture of smectite, disordered I/S, and discrete illite. Increasing temperature favors the formation of illite layers, whether as discrete illite crystals or interstratified within smectite. At fixed temperature, I/S was enriched in illite at a short time, but the proportion of illite layers in I/S decreased with longer reaction times, while discrete illite crystals became more abundant with time (aging). Ammonium concentration also favored the transformation of smectite into illite.

The interaction of the bentonite with ammonium-rich hydrothermal solutions resulted in the uptake of ammonium and the release of initial cations (Na, Ca, Mg) through ion-exchange reactions. The FT-IR spectra of reacted samples showed characteristic bands related to ammonium ions. As reported previously (Shigorova et al., 1981; Higashi, 2000; Busigny et al., 2003), FTIR is a successful approach to estimate NH_4 content. Specifically, the absorption band near 1400 cm^{-1} corresponds to exchangeable NH_4^+ ions within the smectite interlayer, while the band near 1430 cm^{-1} is attributed to non-exchangeable NH_4^+ ions, which are hydrogen-bonded to the high-charge (illite) interlayer (Chourabi and Fripiat, 1981; Petit et al., 1999; Nieto, 2002; Pironon et al., 2003; Šucha et al., 2007). These results suggest that ammonium uptake precedes the smectite-to-illite transformation. In EG solvated samples, the XRD traces expanded to spacings <17 Å, consistent with the presence of disordered I/S. The 001 basal spacing at 16.6–16.9 Å at 150 and 200 °C in EG decreased to 12.7–16.4 Å at 100 °C, reflecting an increasing number of illite layers in I/S and a decrease of discrete smectite layers at 100 °C, and this fact is corroborated by the decrease of the (001) basal spacing observed in patterns of random oriented powder (Figs. 1 and 2). At 100 °C illite layers initially formed as interstratified within smectite layers, but increasing temperature and time favored the formation of discrete illite. The amount of NH_4 ions within the smectite and illite structures supported that, under our experimental conditions, the greatest transformation of smectite into illite was observed at 200 °C and 90 days of reaction, including formation of I/S with a NH_4 content of 0.83 apfu (Table 3), in addition to discrete illite.

The textural observations from TEM align with the XRD analysis, indicating that as temperature and reaction time increase, there is a trend toward greater % illite layers and greater order. Specifically, observations show that the smectite particles increased in thickness from 25 nm up to 120 nm, as well as in the number of layers from <10 to >30 and in crystal length; they also became less wavy in appearance, and the presence of lattice defects decreased. Additionally, the formation of illite layers within smectite crystals produces I/S and eventually discrete illite. These I/S are generally disordered, and they may consist of single layers or multi-layered packets of illite.

The illitization of smectite takes place through a reaction front 12–15 Å smectite layers transition laterally to 10 Å illite layers. For this transformation to take place, the composition of smectite 2:1 layers likely has to change; Si and Al^{VI} concentrations are reduced, while Al^{IV} and Mg^{VI} concentrations increase, as would NH_4^+ (or K^+) contents. This process is similar to the one proposed by Ahn and Peacor (1986). TEM images reveal on numerous occasions this process, which also leads to a decrease in lattice defects as well as an increase in domain size and crystals thickness, both for smectite as well as I/S and illite. This

transformation is a heterogeneous process that takes place by local-scale rearrangement or dissolution/precipitation reactions. Consequently, the observed textures show the progressive transformation of smectite, leading to the formation of interstratified layers of illite and smectite, both as individual packets of these layer types as well as disordered I/S. The presence of an alkaline ammonium solution facilitates the alteration of smectite – as well as accessory phases in the bentonite – and the incorporation of ammonium into the interlayer space, after which structural reorganization is favored by ammonium in the interlayer, helping to stabilize the newly formed high-charge (illite) layers. At 150 and 200 °C, the transformation process is much faster and more widespread, often proceeding through the formation of I/S. As the process advances, thick discrete illite crystals can also form at high temperatures. Overall, this process involves multiple reactions and changes in mineral composition, and the presence of ammonium ions plays a significant role in promoting and stabilizing the transformation from smectite to illite.

Chemical compositions obtained through AEM analysis of individual particles are consistent with this transformation scheme. The synthetic samples show variable morphologies and structural characteristics of particles different from untreated smectites flakes: a) thin particles typically contain lower Si (about 3.4 apfu) and higher Al^{IV} and K or NH_4 content, and their chemical analysis is characteristic of illitic phases; b) scarcer thicker stacks show similar compositions to the starting smectite, but with the incorporation of NH_4 as an interlayer cation. AEM data were plotted in a pyrophyllite-celadonite-muscovite ternary plot, where open symbols correspond to smectite crystals and solid symbols stand for I/S particles (Fig. 9). Two distinct trends can be observed: 1) The alteration of smectite produces an increase in the celadonite component by substitution of Mg^{VI} replacing Al^{VI}, and an increase in the octahedral charge; 2) the I/S particles show a trend toward increase in the muscovite component, characterized by higher Al^{IV} content and tetrahedral charge. Although the scattering of the data slightly blurred the effect of temperature, temperature enhanced the increase in octahedral charge (trend 1), but the dependence of the increase in tetrahedral charge on temperature is a more diffuse trend and would require a larger data set than is available here (trend 2). These overall trends in the smectite-to-illite reaction can also be observed by analyzing the correlations between the different cations (Fig. S5). The transformation of smectite to illite leads to a decrease of Si content, highly correlated with the increase of ammonium and total charge, as well as the increase of octahedral Mg, which correlates positively with the increase of total charge.

The conversion of smectite to illite-smectite (I/S), and then to illite, commonly occurs as a response to burial and is mainly controlled by temperature, pressure, time and system chemistry. In this study temperature and alkaline NH_4 solution appear to be the primary parameters controlling the overall reaction of smectite layers to illite layers, which led to both direct precipitation of illite layers as well as lateral layer replacement by local rearrangement. Given that the formation of ammonium illite is often closely linked to evolution of organic matter in burial sedimentary environments – a process often associated with hydrocarbon maturation in diagenetic settings (e.g. Williams and Ferrell, 1991) or with coal formation in anchizone settings (e.g. Šucha et al., 1998) – improved knowledge of the factors controlling the reaction of smectite to NH_4-bearing I/S and illite are important for understanding cycling of nitrogen in these settings. Results from this study document the influence of temperature, time, NH_4 content and changing crystal chemistry as part of a multi-stage process from initial adsorption of interlayer NH_4 to fixation of NH_4 in interlayers as smectite layers transform to I/S then illite.

5. Concluding remarks

The transformation from smectite to NH_4-illite under experimental conditions of slightly alkaline hydrothermal solutions enriched in ammonium indicate that the reaction is triggered by ammonium adsorption at the interlayer spaces in smectite crystals. Simultaneously, smectite dissolves and releases Si and Al to solution. At the nanometric scale, the dissolution of smectite and the fixation of ammonium ions lead to a layer-by-layer conversion of smectite into illite. This transformation results in an increase of Al^{IV} and Mg^{VI} content within the illitic layers and the formation of disordered I/S structures.

Furthermore, individual illite crystals are formed by precipitation from solution, which is more pronounced at 150 and 200 °C compared to 100 °C. These illite crystals also incorporate interlayered ammonium ions. Our experimental findings indicate that, under moderate temperature conditions, ammonium ions play crucial role in stabilizing the newly forming illite layers and promoting the smectite-to-illite reaction. This transformation process is further enhanced by temperature increase, prolonged reaction times, and increased ammonium concentrations.

CRediT authorship contribution statement

María Bentabol: Writing – review & editing, Writing – original draft, Methodology, Investigation, Conceptualization. **Daniel Lamarca-Irisarri:** Methodology, Investigation. **Alexander E.S. Van Driessche:** Writing – review & editing, Writing – original draft, Validation. **Peter C. Ryan:** Writing – review & editing, Validation. **F. Javier Huertas:** Writing – review & editing, Writing – original draft, Validation, Methodology, Funding acquisition, Conceptualization.

Declaration of competing interest

The authors declare that they have no known competing financial interests or personal relationships that could have appeared to influence the work reported in this paper.

Data availability

The data have been included either in the main text or in the supplementary material. Further specifications on the methodology and/or results will be made available upon request.

Acknowledgments

Financial support was obtained from MINECO (CGL2011-22567, CGL2014-55108P), with contribution of FEDER funds. The authors thank E. Flores for assistance with XRD and FTIR, and M. Mar Abad (CIC-University of Granada) and M. Angeles Laguna (SAI-University of Zaragoza) for expertise with TEM and AEM. F. Nieto (University of Granada) is acknowledged for advice concerning electron microscopy. We appreciate the suggestions provided by anonymous reviewers that substantially improved the final version. FJH, amdg.

Appendix A. Supplementary data

Supplementary data to this article can be found online at https://doi.org/10.1016/j.clay.2024.107478.

References

Ahn, J.H., Peacor, D.R., 1986. Transmission and analytical electron microscopy of Smectite-to-Illite transition. Clay Clay Miner. 34, 165–179.
Altaner, S.P., Ylagan, R.F., 1997. Comparison of structural models of mixed-layer illite/smectite and reaction mechanisms of smectite illitization. Clay Clay Miner. 45, 517–533.
Amouric, M., Olives, J., 1991. Illitization of smectite as seen by high-resolution transmission electron microscopy. Eur. J. Mineral. 3, 831–835.
Barman, A.K., Varadachari, C., Ghosh, K., 1992. Weathering of silicate minerals by organic acids. I. Nature of cation solubilization. Geoderma 53, 45–63.

Bates, S.T., Berg-Lyons, D., Caporaso, J.G., Walters, W.A., Knight, R., Fierer, N., 2011. Examining the global distribution of dominant archaeal populations in soil. Int. Soc. Microb. Ecology J. 5, 908–917.
Bauluz, B., Nieto, F., 2018. Ammonium-bearing micas in very low-grade metapelites: micro- and nano-texture and composition. Clay Miner. 53, 105–116.
Bauluz, B., Subias, I., 2010. Coexistence of pyrophyllite, I-S, R1 and NH_4^+-rich illite in Silurian black shales (Sierra de Albarracín, NE Spain): metamorphic *vs.* hydrothermal origin. Clay Miner. 45, 383–392.
Bethke, C.M., Altaner, S.P., 1986. Layer-by-layer mechanism of smectite illitization and application to a new rate law. Clay Clay Miner. 34, 136–145.
Bobos, I., 2012. Characterization of smectite to NH_4-illite conversion series in the fossil hydrothermal system of Harghita Bai, East Carpathians, Romania. Am. Mineral. 97, 962–982.
Busigny, V., Cartigny, P., Philippot, P., Javoy, M., 2003. Ammonium quantification in muscovite by infrared spectroscopy. Chem.Geol. 198, 21–31.
Caballero, E., Fernández Porto, M.J., Linares, J., Huertas, F., Reyes, E., 1983. Las bentonitas de la Serrata de Níjar (Almería). Mineralogía, geoquímica y mineralogénesis. Estud. Geol. 39, 121–140.
Caballero, E., Jiménez de Cisneros, C., Huertas, F.J., Huertas, F., Pozzuoli, A., Linares, J., 2005. The bentonites from Cabo de Gata, Almería, Spain: a mineralogical and geochemical overview. Clay Miner. 40, 383–426.
Carman, R., Rahm, L., 1997. Early diagenesis and chemical characteristics of interstitial water and sediments in the deep deposition bottoms of the Baltic proper. J. Sea Res. 37, 25–47.
Champness, P.E., Cliff, G., Lorimer, G.W., 1981. Quantitative analytical electron microscopy. Bull. Mineral. 104, 236–240.
Chourabi, B., Fripiat, J.J., 1981. Determination of tetrahedral substitutions and interlayer surface heterogeneity from vibrational spectra of ammonium in smectites. Clay Clay Miner. 29, 260–268.
Cliff, G., Lorimer, G.W., 1975. The quantitative analysis of thin specimens. J. Microsc. 103, 203–207.
Collins, A.G., 1975. Chapter 7. Origin of Oilfield Waters. In: Collins, A.G. (Ed.), Developments in Petroleum Science. Elsevier, pp. 193–252.
Cuadros, J., Altaner, S., 1998a. Compositional and structural features of the octahedral sheet in mixed-layer illite-smectite from bentonites. Eur. J. Mineral. 10, 111–124.
Cuadros, J., Altaner, S., 1998b. Characterization of mixed-layer illite-smectite from bentonites using microscopic, chemical, and X-ray methods: Constraints on the smectite-to-illite transformation mechanism. Am. Mineral. 83, 762–774.
Cuadros, J., Linares, J., 1996. Experimental kinetic study of the smectite-to-illite transformation. Geochim. Cosmochim. Acta 60, 439–453.
Díaz Pinthier, M., 1999. Etude des Interactions Cations Compensateurs/Feuillets Dans Les Argiles: Contribution a La Connaissance Des Mecanismes De Retention Selective. PhD Dissertation,. University of Orleans, p. 233.
Dong, H., 2005. Interstratified Illite-smectite: a review of contributions of TEM data to crystal chemical relations and reaction mechanisms. Clay Sci. 1, 6–12.
Dong, H., Peacor, D.R., Freed, R.L., 1997. Phase relations among smectite, R1 illite-smectite, and illite. Am. Mineral. 82, 379–391.
Drever, J.L., Stillings, L.L., 1997. The role of organic acids in mineral weathering. Colloids Surfaces A 120, 167–181.
Drits, V.A., Srodon, J., Eberl, D.D., 1997a. XRD measurement of mean crystallite thickness of illite and illite/smectite: reappraisal of the Kubler index and the scherrer equation. Clay Clay Miner. 45, 461–475.
Drits, V.A., Lindgreen, H., Salyn, A.L., 1997b. Determination of the content and distribution of fixed ammonium in Illite-smectite by X-ray diffraction: application to North See illite-smectite. Am. Mineral. 82, 79–87.
Drits, V.A., Sakharov, B.A., Salyn, A.L., Lindgreen, H., 2005. Determination of the content and distribution of fixed ammonium in illite-smectite using a modified X-ray diffraction technique: application to oil source rocks of western Greenland. Am. Mineral. 90, 71–84.
Eberl, D., 1978. The reaction of montmorillonite to mixed-layer clay: the effect of interlayer alkali and alkaline earth cations. Geochim. Cosmochim. Acta 42, 1–7.
Eberl, D.D., Srodon, J., Kralik, M., Taylor, B.E., Peterman, Z.E., 1990. Ostwald ripening of clays and metamorphic minerals. Science 248, 474–477.
Fang, Q., Churchman, G.J., Hong, H., Chen, Z.Q., Liu, J., Yu, J., Han, W., Wang, C., Zhao, L., Furnes, H., 2017. New insights into microbial smectite illitization in the Permo-Triassic boundary K-bentonites, South China. Appl. Clay Sci. 140, 96–111.
Farmer, V.C., 1974. The layer silicates. In: The Infrared Spectra of Minerals. Mineralogical Society of Great Britain and Ireland, pp. 331–365.
Ferrage, E., Vidal, O., Mosser-Ruck, R., Cathelineau, M., 2011. A reinvestigation of smectite illitization in experimental hydrothermal conditions: results from X-ray diffraction and transmission electron microscopy. Am. Mineral. 96, 207–223.
Froelich, P.N., Klinkhammer, G.P., Bender, M.L., Luedtke, N.A., Heath, G.R., Cullen, D., Dauphin, P., Hammond, D., Hartman, B., Maynard, V., 1979. Early oxidation of organic matter in pelagic sediments of the eastern equatorial Atlantic: suboxic diagenesis. Geochim. Cosmochim. Acta 43, 1075–1090.
Gautier, M., Muller, F., Beny, J.M., Guegan, R., 2010. NH_4-smectite: characterization, hydration properties and hydro mechanical behavior. Appl. Clay Sci. 49, 247–254.
Harlov, D.E., Andrut, M., Potër, B., 2001. Characterisation of tobelite $(NH_4)Al_2[AlSi_3O_{10}](OH)_2$ and ND_4-tobelite $(ND_4)Al_2[AlSi_3O_{10}](OD)_2$ using IR spectroscopy and Rietveld refinement of XRD spectra. Phys. Chem. Miner. 28, 268–276.
Higashi, S., 1982. Tobelite, a new ammonium dioctahedral mica. Mineral. J. 424, 138–146.
Higashi, S., 2000. Ammonium-bearing mica and mica/smectite of several pottery stone and pyrophyllite deposits in Japan: their mineralogical properties and utilization. Appl. Clay Sci. 16, 171–184.
Huang, W.J., 1993. The formation of illitic clays from kaolinite in KOH solutions from 225°C to 350°C. Clay Clay Miner. 41, 645–654.
Huang, W.L., Bishop, A.M., Brown, R.W., 1986. The effect of fluid/rock ratio on feldspar dissolution and illite formation under reservoir conditions. Clay Miner. 21, 585–601.
Huertas, F.J., Cuadros, J., Linares, J., 1995. Modelling of potassium exchange in a natural, polyionic montmorillonite under hydrothermal conditions. Appl. Geochem. 10, 347–355.
Huertas, F., Fuentes-Cantillana, J.L., Jullien, F., Rivas, P., Linares, J., Fariña, P., Ghoreychi, M., Jockwer, N., Kickmaier, W., Martínez, M.A., Samper, J., Alonso, E., Elorza, F.J., 2000. Full-Scale Engineered Barriers Experiment for a Deep Geological Repository for High-Level Radioactive Waste in Crystalline Host Rock (FEBEX Project). European Commission, EUR 19147EN, Brussels.
Inoue, A., 1983. Potassium fixation by clay minerals during hydrothermal treatment. Clay Clay Miner. 31, 81–91.
Inoue, A., Lanson, B., Marques-Fernandes, M., Sakharov, B., Murakami, T., Meunier, A., Beaufort, D., 2005. Illite-smectite mixed-layer minerals in hydrothermal alteration of volcanic rocks: I. One-dimensional XRD structure analysis and characterisation of component layers. Clay Clay Miner. 53, 423–439.
Inoue, A., Watanabe, T., Kohyama, N., Brusewitz, A.M., 1990. Characterization of illitization of smectite in bentonite beds at Kinnekulle, Sweden. Clay Clay Miner. 38, 241–249.
Jo, J., Yamanaka, T., Kashimura, T., Okunishi, Y., Kuwahara, Y., Kadotoa, I., Miyoshi, Y., Ishibashi, J., Chiba, H., 2018. Mineral nitrogen isotope signature in clay minerals formed under high ammonium environment conditions in sediment associated with ammonium-rich sediment-hosted hydrothermal system. Geochem. J. 52, 317–333.
Lanson, B., Sakharov, B.A., Claret, F., Drits, V.A., 2009. Diagenetic smectite-to-illite transition in clay-rich sediments: a reappraisal of X-ray diffraction results using the multi-specimen method. Am. J. Sci. 309, 476–516.
Lawrence, C., Harden, J., Maher, K., 2014. Modeling the influence of organic acids on soil weathering. Geochim. Cosmochim. Acta 139, 487–507.
Leone, G., Reyes, E., Cortecci, G., Pochini, A., Linares, J., 1983. Genesis of bentonites from Cabo de Gata, Almería, Spain: a stable isotope study. Clay Miner. 18, 227–238.
Lindgreen, H., Hansen, P.L., 1991. Ordering of illite-smectite in upper Jurassic claystones from the North Sea. Clay Miner. 26, 105–125.
McCarty, D.K., Sakharov, B.A., Drits, V.A., 2009. New insights into smectite illitization: a zoned K-bentonite revisited. Am. Mineral. 94, 1653–1671.
Moore, D.M., Reynolds, R.C. Jr, 1997. X-Ray Diffraction and Identification and Analysis of Clay Minerals, Second ed. Oxford University Press, Oxford.
Mosser-Ruck, R., Cathelineau, M., Baronnet, A., Trouiller, A., 1999. Hydrothermal reactivity of K-smectite at 300 °C and 100 bar: dissolution-crystallization process and non-expandable dehydrated smectite formation. Clay Miner. 34, 275–290.
Mosser-Ruck, R., Pironon, J., Cathelineau, M., Trouiller, A., 2001. Experimental illitization of smectite in a K-rich solution. Eur. J. Mineral. 13, 829–840.
Murakami, T., Inoue, A., Lanson, B., Meunier, A., Beaufort, D., 2005. Illite-smectite mixed-layer minerals in the hydrothermal alteration of volcanic rocks: II. One-dimensional HRTEM structure images and formation mechanisms. Clay Clay Miner. 53, 440–451.
Nadeau, P.H., Wilson, M.J., McHardy, W.J., Tait, J.M., 1985. The conversion of smectite to illite during diagenesis: evidence from some illitic clays from bentonites and sandstones. Mineral. Mag. 49, 393–400.
Nieto, F., 2002. Characterization of coexisting NH_4- and K-micas in very low-grade metapelites. Am. Mineral. 87, 205–216.
Petit, S., Righi, D., Madejová, J., Decarreau, A., 1998. Layer charge estimation of smectites using infrared spectroscopy. Clay Miner. 34, 579–591.
Petit, S., Righi, D., Madejová, J., Decarreau, A., 1999. Interpretation of the infrared NH_4^+ spectrum of the NH_4^+-clays: application to the evaluation of the layer charge. Clay Miner. 34, 543–549.
Petit, S., Righi, D., Madejová, J., 2006. Infrared spectroscopy of NH_4^+-bearing and saturated clay minerals: a review of the study of layer charge. Appl. Clay Sci. 34, 22–30.
Petit, S., Decarreau, A., Grégoire, B., Ferrage, E., 2023. Generalized relationships between the ionic radii of octahedral cations and the *b* crystallographic parameter of clays and related minerals. Clay Miner. 58, 143–194.
Pironon, J., Pelletier, M., De Donato, P., Mosser-Ruck, R., 2003. Characterization of smectite and illite by FTIR spectroscopy of interlayer NH_4^+ cations. Clay Miner. 38, 201–211.
Radoslovich, E.W., 1960. The structure of muscovite. Acta Crystallogr. 13, 919–932.
Roberson, H., Lahann, R., 1981. Smectite to illite conversion rates: effects of solution solution chemistry. Clay Clay Miner. 29, 129–135.
Ruiz Cruz, M.D., Sanz de Galdeano, C., 2008. High-temperature ammonium white mica from the Betic Cordillera (Spain). Am. Mineral. 93, 977–987.
Shigorova, T.A., Kotov, N.V., Kotelnikova, Y.N., Shmakin, B.M., Frank-Kamenestskiy, V. A., 1981. Synthesis, diffractometry, and IR spectroscopy of micas in the series from muscovite to the ammonium analog. Geochem. Int. 18, 76–82.
Środoń, J., 2010. Evolution of boron and nitrogen content during illitization of bentonites. Clay Clay Miner. 58, 743–756.
Šucha, V., Elsass, F., Eberl, D.D., Kuchta, L., Madejová, J., Gates, W.P., Komadel, P., 1998. Hydrothermal synthesis of ammonium illite. Am. Mineral. 83, 58–67.
Šucha, V., Uhlík, P., Madejová, J., Petit, S., Kraus, I., Puškelová, L., 2007. Particle properties of hydrothermal ammonium-bearing illite-smectite. Clay Clay Miner. 55, 36–44.
Surdam, D.C., Crossey, L.J., Hagen, E.S., Heasler, H.P., 1989. Organic-inorganic interactions and sandstone diagenesis. Am. Assoc. Pet. Geol. Bull. 73, 1–23.
Vazquez, M., Bauluz, B., Nieto, F., Morata, D., 2016. Illitization sequence controlled by temperature in volcanic geothermal systems: the Tinguiririca geothermal field, Andean Cordillera, Central Chile. Appl. Clay Sci. 134, 221–234.

Wakakita, R., Saito, A., Sakuma, H., Anraku, S., Kikuchi, R., Otake, T., Sato, T., 2023. Difference in expansion and dehydration behaviors between NH_4- and K-montmorillonite. Appl. Clay Sci. 231, 106722.
Whitney, G., Velde, B., 1993. Changes in particle morphology during illitization: an experimental study. Clay Clay Miner. 41, 209–218.
Williams, L.B., Ferrell, R.E., 1991. Ammonium substitution in illite during maturation of organic matter. Clay Clay Miner. 39, 400–408.
Williams, L.B., Ferrell, R.E., Chinn, E.W., Sassen, R., 1989. Fixed-ammonium in clays associated with crude oils. Appl. Geochem. 4, 605–616.
Williams, L.B., Wilcoxon, B.R., Ferrell, R.E., Sassen, R., 1992. Diagenesis of ammonium during hydrocarbon maturation and migration, Wilcox Group, Louisiana, U.S.a. Appl. Geochem. 7, 123–134.
Yamamoto, T., 1967. Mineralogical studies of sericite associated with Roseki ores in the western part of Japan. Mineral. J. 5, 77–97.